The temporal resolution of the voltage clamp (4 μs) is limited by the rise time of the voltage pulse step applied to the amplifier. The capacitance feedback was reset just before the onset of all signals presented. A small, rising slope in charge transfer records, corresponding to a steady-state current, was subtracted from all records presented. This current probably corresponds to a low rate of pump cycling during which three cytoplasmic Na ions are exchanged for two extracellular Na ions (*16*). All results were obtained at 37°C. Membrane capacitance was determined as the difference between pipette capacitance with the intact membrane patch and the capacitance after patch rupture with subsequent formation of a hydrocarbon (hexane) meniscus, about 1 μm in thickness, across the pipette orifice. The extracellular (pipette) solution contained 120 mM Na-[2-(*N*-mortholino)ethanesulphonic] acid (MES), 0.5 mM $MgCl_2$, 15 mM *N*-methylglucamine (NMG)–Cl, 10 mM tetraethylammonium (TEA), 10 mM MES, 5 mM EGTA, and 15 mM Hepes, set to pH 7.0 with additional NMG. For the cytoplasmic solution and for pipette solutions with varied Na concentrations, Na-MES was replaced with NMG-MES.
8. W. Stürmer, R. Bühler, H.-J. Apell, P. Läuger, *J. Membr. Biol.* **121**, 163 (1991).
9. R. Goldshleger, S. J. D. Karlish, A. Rephaeli, W. D. Stein, *J. Physiol.* **387**, 331 (1987); K. Fendler, E. Grell, E. Bamberg, *FEBS Lett.* **224**, 83 (1987).
10. R. F. Rakowski, *J. Gen. Physiol.* **101**, 117 (1993).
11. All Na,K pump charge movements defined in this way were completely absent when 100 μM ouabain was included in the pipette (that is, on the extracellular side). With 120 mM extracellular Na, 1 μM ouabain completely abolished charge movements.
12. Nearly identical results were obtained by the subtraction of signals after the removal of cytoplasmic Na. Very similar results were also obtained when high cytoplasmic PO_4 (4 mM) and Mg (4 mM) were applied to induce the E_2 pump conformation, and records taken after the removal of PO_4 were subtracted.
13. S. Heyse, I. Wuddel, H.-J. Apell, W. Stürmer, *J. Gen. Physiol.*, in press.
14. This process requires that the membrane electrical field falls off along the diffusion pathway of the Na ion (that is, the access channel). The position and profile of the membrane field along such a channel, closed at one end, depend minimally on the unknown physical (dielectric) properties of the membrane protein and the geometry of the pore. It seems safe to assume that if the pore is so narrow that water is structured (or bound) within the pore, then membrane potential will fall off along its length. This relation can be assumed for the E_2P3N state. If the channel is wider and the dielectric properties of the transporter protein are more like those of membrane than of water, then the electrical field will be forced out of the water-filled pore and into a position through its closed end. This relation can be assumed for the E_2P2N state.
15. C. A. Vandenberg, *Proc. Natl. Acad. Sci. U.S.A.* **84**, 2560 (1987); L. Nowak, P. Bregestovski, P. Ascher, A. Herbet, A. Prochiantz, *Nature* **307**, 462 (1984).
16. K. H. Lee and R. Blostein, *Nature* **285**, 338 (1980).
17. D. W. Hilgemann, K. D. Philipson, D. A. Nicoll, *Biophys. J.* **61**, A390 (1992).
18. L. A. Vasilets and W. Schwarz, *J. Membr. Biol.* **91**, 43 (1990).
19. R. F. Rakowski, L. A. Vasilets, J. La Tona, W. Schwarz, *ibid.* **121**, 177 (1991).
20. I thank G. A. Frazier and Texas Instruments for designing and building the data acquisition–pulse generator system used in these experiments; R. Lobdill and Axon Instruments for advice and modifying the patch clamp used; P. Foley for technical assistance; V. V. Golobov for mathematical advice; and D. C. Gadsby, R. A. Levis, M. Weber, S. Matsuoka, and K. D. Philipson for helpful discussions. Supported by grants from the American Heart Association and the National Institutes of Health. This work has been reported in part in abstract form (*17*).

20 October 1993; accepted 14 January 1994

Crystal Structures at 2.5 Angstrom Resolution of Seryl-tRNA Synthetase Complexed with Two Analogs of Seryl Adenylate

Hassan Belrhali, Anna Yaremchuk, Michael Tukalo, Kjeld Larsen, Carmen Berthet-Colominas, Reuben Leberman, Barbro Beijer, Brian Sproat, Jens Als-Nielsen, Gerhard Grübel, Jean-François Legrand, Mogens Lehmann, Stephen Cusack*

Crystal structures of seryl-tRNA synthetase from *Thermus thermophilus* complexed with two different analogs of seryl adenylate have been determined at 2.5 Å resolution. The first complex is between the enzyme and seryl-hydroxamate–AMP (adenosine monophosphate), produced enzymatically in the crystal from adenosine triphosphate (ATP) and serine hydroxamate, and the second is with a synthetic analog of seryl adenylate (5′-*O*-[*N*-(L-seryl)-sulfamoyl]adenosine), which is a strong inhibitor of the enzyme. Both molecules are bound in a similar fashion by a network of hydrogen bond interactions in a deep hydrophilic cleft formed by the antiparallel β sheet and surrounding loops of the synthetase catalytic domain. Four regions in the primary sequence are involved in the interactions, including the motif 2 and 3 regions of class 2 synthetases. Apart from the specific recognition of the serine side chain, the interactions are likely to be similar in all class 2 synthetases.

Aminoacyl-tRNA synthetases specifically attach amino acids to the 3′-adenosine of their cognate tRNAs in a two-step reaction. In the presence of Mg^{2+} and ATP, the enzyme first activates the amino acid to form the enzyme-bound aminoacyl-adenylate intermediate. In the second step, the amino acid is ligated to the cognate tRNA. The 20 aminoacyl-tRNA synthetases are divided into two classes of ten (*1, 2*). The two classes are characterized by different short sequence motifs and have quite different catalytic domain topologies, the Rossmann fold for class 1 and an antiparallel β fold for class 2 (*3*). For class 1 synthetases, crystal structures of complexes with ATP have been described for methionyl-tRNA synthetase (MetRS) (*4*) and GlnRS (*5*), with the amino acid alone for TyrRS (*6*) and with the aminoacyl-adenylate for TyrRS (*7*) and TrpRS (*8*). A catalytic pathway for the amino acid activation has been proposed for TyrRS (*9*) and GlnRS (*10*). For class 2 synthetases, preliminary results have been given for the ATP binding site (*11–13*), but no structural information is available for the amino acid binding site.

The crystal structures of seryl-tRNA synthetase from *T. thermophilus* complexed with two different seryl-adenylate analogs described here reveal the aminoacyl-adenylate binding site and the role of several of the conserved residues in class 2 aminoacyl-tRNA synthetases. The first complex was obtained by soaking native crystals of the enzyme with ATP and serine hydroxamate (SerHx, $^{+}H_3N$-HCR-CO-N(H)OH, where R is the serine side chain). SerHx inhibits growth in *Escherichia coli* and has been described as a competitive inhibitor of the enzyme toward the amino acid (*14*). The crystallographic data reveal strong difference electron density for a serine hydroxamate-AMP (SerHx-AMP) molecule (Fig. 1C). The enzymatic activation of serine hydroxamate has subsequently been confirmed by biochemical studies (see below). Ueda *et al.* (*15*) have described a synthetic alanyl-adenylate analog (5′-O-[*N*-(L-alanyl)-sulfamoyl]adenosine) and showed that it was an inhibitor of alanyl-tRNA synthetase activity. Following this idea, we have synthesized the corresponding seryl compound, 5′-O-[*N*-(L-seryl)-sulfamoyl]adenosine (Fig. 1B) and have co-crystallized it with *T. thermophilus* seryl-tRNA synthetase (*16*). This second structure confirms the location of the seryl-adenylate binding site and comparisons with the first structure indicate that the two analogs do not have the same length linkage

H. Belrhali, A. Yaremchuk, M. Tukalo, K. Larsen, C. Berthet-Colominas, R. Leberman, S. Cusack, EMBL Grenoble Outstation, c/o ILL, BP 156, 38042 Grenoble Cedex 9, France.
B. Beijer and B. Sproat, Biochemical Instrumentation Programme, EMBL, Meyerhofstrasse 1, Postfach 10.2209, D-69012 Heidelberg, Germany.
J. Als-Nielsen, G. Grübel, J-F. Legrand, M. Lehmann, European Synchrotron Radiation Facility, BP 220, F-38043 Grenoble Cedex, France.

*To whom correspondence should be addressed.

between the phosphate or sulfamoyl group and the amino acid (Fig. 1).

Crystals of native seryl-tRNA synthetase from *T. thermophilus*, grown as described (*16*) were soaked for 15 hours in a freshly prepared solution of 10 mM ATP (sodium salt; Boehringer) and 20 mM D,L-serine hydroxamate racemic mixture (Sigma). Diffraction data were measured with a 180-mm Mar Research image-plate detector on the wiggler beamline W32 at LURE (*17*), and the data were integrated with the MOSFLM package (*18*). The starting model for refinement with X-PLOR (*19*) was the structure of the native enzyme without ligand (*21*). The initial *R* factor of 39.8% was reduced to 26.6% by rigid-body refinement and subsequently to 20.7% by a simulating annealing run, followed by 150 cycles of conjugate gradient energy minimization. A difference map calculated with the program SIGMAA (*22*) revealed strong additional electron density (>14 σ) in each monomer active site and was easily identifiable as an AMP molecule with additional density beyond the phosphate group. Two AMP molecules were then included in the model and, after further cycles of energy minimization, the new difference map (Fig. 2) permitted the seryl hydroxamate (SerHx) moiety to be built into one of the crystallographically independent active sites with a linkage of the form adenosine-Pα-O-N(H)-CO-CHR-NH3$^+$. The geometry of the hydroxamate group was taken from the structure of ammonium oxalohydroxamate (*22*) with the six atoms O-N(H)-CO-C being coplanar. The final model comprising the synthetase dimer with a single SerHx-AMP, a single AMP and 130 water molecules had an *R* factor of 17.6% (Table 1).

5′-O-[*N*-(L-seryl)-sulfamoyl]adenosine was synthesized by a method analogous to that described for the alanyl compound (*15*) except that 2′,3′-O-isopropylidene-5′-O-sulfamoyladenosine was reacted with the *N*-hydroxysuccinimide ester of *t*-butoxycarbonyl-L-serine benzyl ether [Boc-Ser(Bzl)-OSu]. The product from this reaction was obtained in about 60% yield after purification by silica gel column chromatography with a gradient of ethanol from 5 to 25% in dichloromethane. The protecting groups were then removed in two stages. The isopropylidene and Boc protecting groups were cleaved with trifluoroacetic acid–water (5:2 v/v) as described (*23*). The remaining benzyl-protected product was purified by chromatography (i) on RP-2 silica and development with water and methanol (3:1 v/v) and (ii) on silica and development with methanol and dichloromethane (1:1 v/v). Finally, the benzyl protecting group of the serine side chain hydroxyl group was removed by hydrogenolysis at atmospheric pressure with 10% palladium on charcoal in methanol and water (1:1 v/v) containing 3% acetic acid. The crude product was purified by chromatography on RP-2 silica and development with methanol and water (1:3 v/v); a final purification was performed by reversed-phase high-performance liquid chromatography on a 4-μm C18 column. The structures of the product and intermediates were confirmed by nuclear magnetic resonance spectroscopy. The inhibition constant (K_i) of Ser-AMS for the *E. coli* enzyme was in the nanomolar range.

Seryl-tRNA synthetase was co-crystallized with 350 μM Ser-AMS. Diffraction data were measured with a 180 mm Mar Research image-plate detector at the European Synchrotron Radiation Facility (ESRF), Grenoble, France. The TROIKA beamline (ID10) was used, which has an undulator insertion device as source and a thin silicon monochromator (*24*). The model was refined as described (Table 1). The final model had an *R* factor of 18.5% and consisted of the synthetase dimer, two Ser-AMS, and 178 water molecules.

The mode of binding of the two adenylate analogs within the active site cleft is similar (Fig. 3). A complete network of hydrogen bonds, including a few bridging water molecules, determines the strong and specific binding of the two molecules (Fig. 4). Four zones of the synthetase are involved, each containing residues highly conserved in all class 2 synthetases (Figs. 3 and 5).

The purine ring of the adenosine stacks on Phe^{275} (motif 2) and, on the opposite side, is in Van der Waals contact with Arg^{386} (motif 3). Adenosine specificity is determined by hydrogen bond interactions to the ring nitrogens (Fig. 4). The Ile^{183} (*8*) in TrpRS and Leu^{261} in GlnRS (*10*) play the same role as Val^{272} in SerRS in providing specificity for ATP by two main chain interactions. Such interactions are apparently absent in MetRS (*4*) and TyrRS (*6*). The ribose ring conformation is C3′-*endo*. The ribose 2′-hydroxyl interacts with the carbonyl oxygen of Thr^{346} and a water molecule, whereas the 3′-hydroxyl bonds with Glu^{345}. The latter residue is in β strand A4 (shown green in Fig. 3), and is also conserved in class 2 synthetases (Fig. 5). The absolutely conserved motif 2 resi-

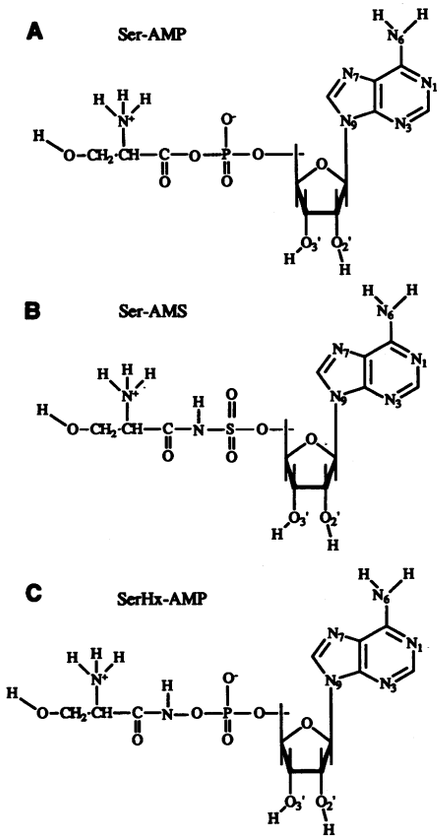

Fig. 1. Structural formulae of (**A**) normal seryl-adenylate (Ser-AMP) and the two analogs Ser-AMS (**B**) and SerHx-AMP (**C**).

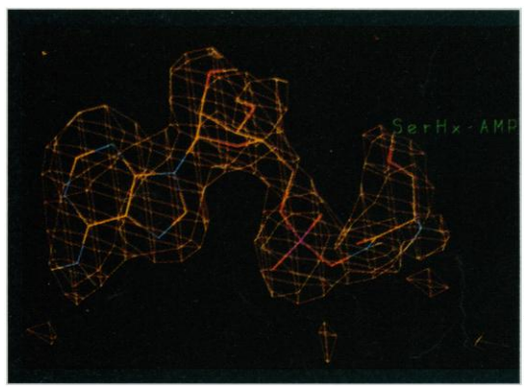

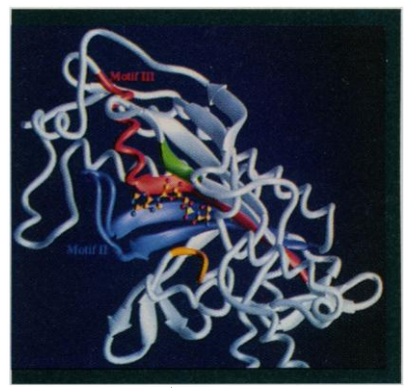

Fig. 2 (left). Omit electron density, contoured at 3σ, for the SerHX-AMP molecule calculated with phases derived from the model at the stage before the serine moiety had been included. **Fig. 3 (right).** Ribbon diagram of the catalytic domain of seryl-tRNA synthetase showing Ser-AMS in the active site. The four zones involved in binding the adenylate are the TXE loop (yellow), motif 2 (blue), β strand A4 (green), and motif 3 (red). The figure was prepared with the program RIBBONS (*29*).

due Arg[256], disordered in the absence of substrates, interacts with the phosphate (sulfamoyl-) group. The serine hydroxyl acts as a hydrogen bond donor to Glu[279] (motif 2) and an acceptor for Thr[380] (motif 3). The amino group is stabilized by hydrogen bonds to Thr[225], Glu[227], and Glu[279]. The binding sites of the two analogs differ only with respect to certain water molecules in the region of the different linkages and an extra hydrogen bond between the carbonyl group and Thr[225] in the SerHx-AMP complex. Superposition of the two adenylate molecules (Fig. 6) shows that the extra bond in the SerHx-AMP molecule [-P-O-N(H)-, instead of -S-N(H)- in Ser-AMS] is accommodated by a small relative shift in the position of the phosphate group leaving the adenosine and serine moieties in the same position.

One unexpected result of these measurements is the observation of seryl-tRNA synthetase catalyzed activation of serine hydroxamate with ATP to form a novel adenylate-like molecule, SerHx-AMP. The formation of an intermediate distinct from the normal seryl-adenylate has been confirmed by biochemical studies (*25*) that show that SerHx-AMP has a higher stability to hydrolysis than Ser-AMP. In addition, ^{31}P NMR studies support the identification of the linkage in this molecule as -P-O-N(H)- rather than -P-N(OH)- (*26*). Surprisingly, the synthetase is able to accommodate the extra bond length in this molecule. Recent results have shown that the SerHx-AMP is a substrate for the second step of aminoacylation reaction (*25*), that is, transfer to tRNA^{Ser}. These observations reopen the question of the exact mechanism of serine hydroxamate inhibition of growth in *E. coli* (*14*).

Apart from the specific recognition of the amino acid side chain, the mode of binding of the adenylate observed here is probably similar in other class 2 synthetases. This follows from the conservation of the interacting residues, which are located in four zones in the synthetase sequence (Fig. 5). The first of these zones is the loop between strand βA2 and helix H9 which brings, in the case of seryl-tRNA synthetases, residues Thr[225] and Glu[227] (T-X-E) into a position to interact with the amino function of the amino acid. One or both of these residues (or the conservative alternatives, serine and glutamine) are in these positions in all class 2 synthetases with the exception of the threonyl-tRNA synthetases. In motif 2, interacting residues are also conserved, particularly the arginine and carboxylic acid of the Phe-Arg[256]-X-Glu peptide before the motif 2 loop, and Phe[275] and Glu[279] after the loop. Binding of either ATP or the adenylate fixes the side-chain conformations of the Arg[256]-X-Glu peptide, and thus it is the first step toward the stabilization of the motif 2 loop that is involved in tRNA acceptor stem interactions. Thus the presence of the intermediate may favor the correct binding of the tRNA in the active site. In the third region, there is a highly conserved glutamic acid (which is glutamine in some synthetases) in strand βA4, which binds the 3′ hydroxyl of the ribose. The 3′-*endo* confor-

Table 1. Crystallographic data on the two adenylate complexes. For the Ser-AMS complex, low resolution data, absent because of detector saturation and a large beam-stop shadow, were measured separately on a second crystal with a laboratory source and the two data sets were merged.

Item	Synthetase + ATP + serine hydroxamate	Synthetase + Ser-AMS (inhibitor)	
Space group	$P2_1$	$P2_1$	
Wavelength (Å)	0.90 (LURE)	0.79(ESRF)	1.54(EMBL)
Crystals (*N*)	3	1	1
Cell parameters			
a (Å)	85.10	86.42	86.18
b (Å)	125.21	126.35	126.35
c (Å)	62.40	62.94	62.77
β (°)	108.8°	109.0°	109.1°
Resolution (Å)	2.50	2.55	3.50
		Combined data	
Data			
Total reflections	170878	217462	
Unique reflections	36920	38589	
Average redundancy	4.6	5.6	
Completeness (%)*	87 (87)	91 (88)	
R_{merge} (%)*	6.6 (16.4)	7.5 (10.9)	
$I > 3\sigma$ (%)*	78 (51)	89 (73)	
Model			
Refinement *R* factor (%)	17.6	18.5	
Rms deviations:			
Bond lengths (Å)	0.016	0.016	
Bond angles (°)	3.3	3.2	
Water molecules	130	178	
Average *B* factor (Å^2)†	25.4, 30.0	17.1, 19.8	

*Highest resolution. †Main chain, side chain.

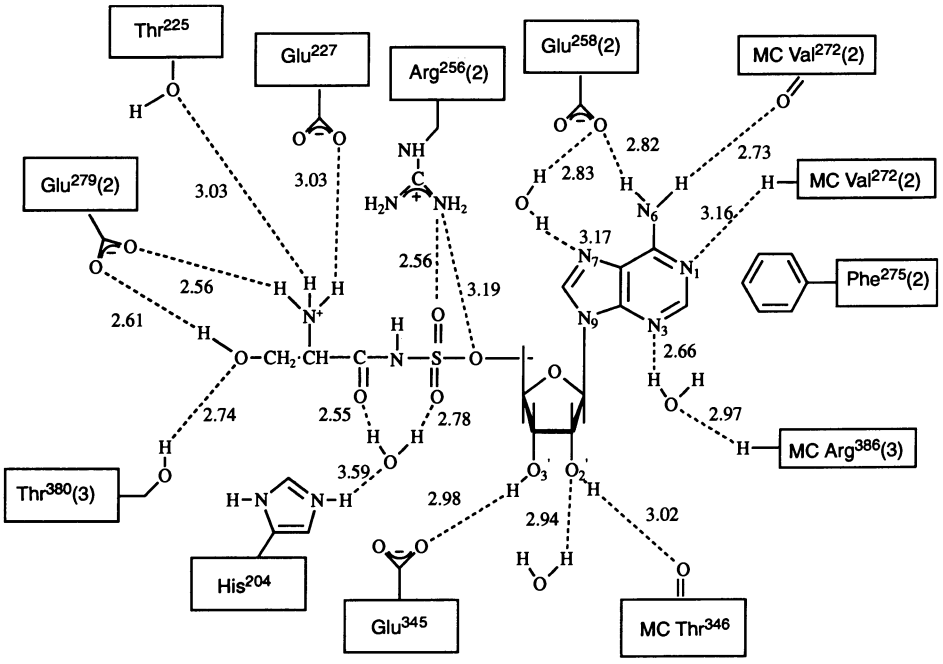

Fig. 4. Diagram of the polar interactions between the Ser-AMS molecule and the synthetase. Residues belonging to motifs 2 and 3 are indicated. Phe[275] is stacked with the purine ring of the adenosine. Distances in angstroms are taken from monomer 2 in the structure.

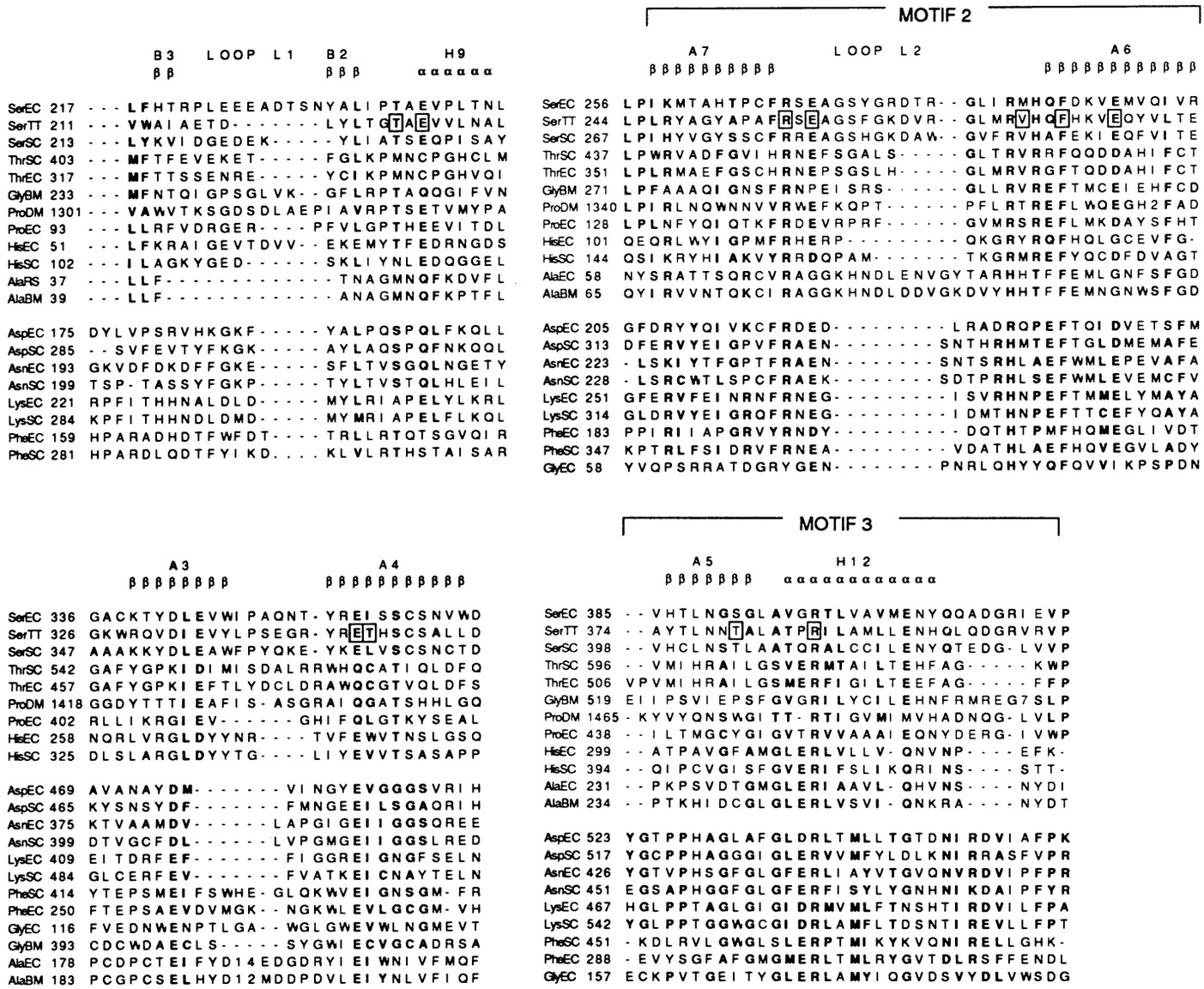

Fig. 5. Alignment of class 2 synthetases in the four zones involved in adenylate binding showing the high conservation of interacting residues (boxed). The figure is adapted from that in (*30*). The secondary structure assignments derived from the *E. coli* seryl-tRNA synthetase structure are indicated. Abbreviations used: SerEC: seryl-tRNA synthetase from *E. coli*, TT: *T. thermophilus*, SC: *Saccharomyces cerevisiae*, HU: human, DM: *Drosophila*, BM: *Bombyx mori*.

mation of the ribose may be a characteristic of the class 2 synthetase ATP-binding site since in class 1 synthetases, the ribose is bound in the 2′-*endo* conformation (*4, 7*). It should be noted that some of the above-cited residues might modify their interactions when the 3′ end of the tRNA is in position for the second step of the aminoacylation reaction.

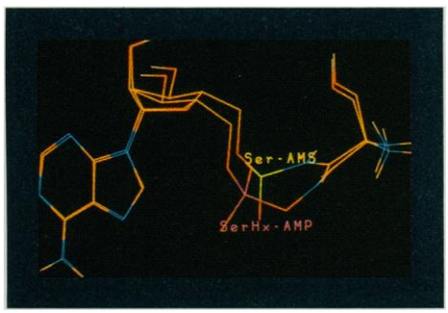

Fig. 6. Superposition of the active site conformations of Ser-AMS and SerHx-AMP.

Serine specificity is guaranteed (i) by two hydrogen bond interactions with the side chain hydroxyl group and (ii) by the size of the binding pocket, which would not allow a larger side chain. The motif 3 residue that takes part in serine recognition, Thr^{380}, is not fully conserved among the seryl-tRNA synthetases; in the *E. coli* enzyme it is Ser^{391}, which however preserves the same functionality. In *E. coli* phenylalanyl-tRNA synthetase, the Ala^{294} in the small subunit, which occupies almost exactly this position in motif 3 (Fig. 5), has been implicated in amino acid specificity for this enzyme (*27*). In the serine binding site, the only other amino acid that could make similar polar interactions is threonine; glycine and alanine would be unfavorable because of the absence of hydrogen bonding capability, and other amino acids would be too large. Model building suggests that discrimination against threonine depends on the fact that its methyl group would be in an unfavorable hydrophilic environment, within 2.5 Å of the main chain carbonyl-oxygen of Ser^{348} and the side chain of Asn^{378}.

An explanation of the catalytic mechanism of serine activation requires further information on the initial binding sites and conformations of the ATP, magnesium,

and amino acid. Crystallographic measurements at 3.1 Å resolution have shown the conformation of ATP soaked into native crystals of *T. thermophilus* seryl-tRNA synthetase and its analog AMPPCP soaked into crystals of the complex with $tRNA^{Ser}$ (*13*). In both cases the triphosphate moiety of ATP was in an extended conformation with the β-phosphate in a position incompatible with the simultaneous binding of the serine as observed in the adenylate complexes. This observation suggests that the initial conformation of the triphosphate in the presence of magnesium and the amino acid is different. This hypothesis is supported by comparison of the two independent active sites in the SerHx-AMP complex. In one active site, a SerHx-AMP molecule is observed as described above. In the other active site the electron density is less well defined but can be interpreted as being a superposition of ATP in a bent conformation and the adenylate product. Recent data at 2.4 Å resolution of a Mn^{2+}-ATP complex with the native synthetase shows the ATP in the bent conformation with the γ-phosphate interacting with the universally conserved Arg^{386} in motif 3 (*28*). The Mn^{2+} ion is coordinated by the ATP α- and β-phosphates as well as Glu^{345} and Ser^{348}, both residues being generally functionally conserved in class 2 synthetases (Fig. 5). This conformation of the ATP, when superimposed on that of the adenylate, is very suggestive of an in-line displacement mechanism for serine activation.

REFERENCES AND NOTES

1. G. Eriani, M. Delarue, O. Poch, J. Gangloff, D. Moras, *Nature* **347**, 203 (1990).
2. D. Moras, *Trends Biochem. Sci.* **17**, 159 (1992).
3. S. Cusack, C. Berthet-Colominas, M. Härtlein, N. Nassar, R. Leberman, *Nature* **347**, 249 (1990).
4. S. Brunie, C. Zelwer, J-L. Risler, *J. Mol. Biol.* **216**, 411 (1990).
5. M. A. Rould, J. J. Perona, D. Söll, T. A. Steitz, *Science* **246**, 1135 (1989).
6. P. Brick and D. M. Blow, *J. Mol. Biol.* **194**, 287 (1987).
7. P. Brick, T. N. Bhat, D. M. Blow, *ibid.* **208**, 83 (1989).
8. S. Doublié, thesis, University of North Carolina (1993).
9. A. Fersht, *Biochemistry* **26**, 8031 (1987).
10. J. J. Perona, M. A. Rould, T. A. Steitz, *ibid.* **32**, 8757 (1993).
11. J. Caverelli, B. Rees, M. Ruff, J-C. Thierry, D. Moras, *Nature* **362**, 181 (1993).
12. S. Cusack *et al.*, in *The Translational Apparatus*, K. H. Nierhaus *et al.*, Eds. (Plenum, New York, 1993), pp. 1–12.
13. V. Biou, A. D. Yaremchuk, M. A. Tukalo, S. Cusack, *Science* **263**, 1404 (1994).
14. T. Tosa and L. I. Pizer, *J. Bacteriol.* **106**, 966 and 972 (1971).
15. H. Ueda *et al.*, *Biochim. Biophys. Acta* **1080**, 126 (1991).
16. M. B. Garber *et al.*, *J. Mol. Biol.* **213**, 631 (1990).
17. R. Fourme *et al.*, *Rev. Sci. Inst.* **63**, 982 (1992).
18. A. G. W. Leslie, Joint CCP4 and ESF-EACBM Newsletter on Protein Crystallography, No. 26 (April 1992), Daresbury Laboratory, Warrington WA4 4AD, England.
19. A. T. Brünger, *X-PLOR Version 3.1* (Yale Univ. Press, New Haven, CT, 1993).
20. M. Fujinaga, C. Berthet-Colominas, A. D. Yaremchuk, M. A. Tukalo, S. Cusack, *J. Mol. Biol.* **234**, 222 (1993).
21. R. J. Read, *Acta Crystallogr. A* **42**, 140 (1986).
22. A. Sameena Begum, V. K. Jain, S. Ramakumar, C. L. Khetrapal, *ibid.* **C44**, 1047 (1988).
23. J. Castro-Pichel, M. T. Garcia-Lopez, F. G. Delas Heras, *Tetrahedron* **43**, 383 (1987).
24. M. S. Lehmann, J. Als-Nielsen, G. Grübel, J-F. Legrand, Joint CCP4 and ESF-EACBM Newsletter on Protein Crystallography, No. 28 (May 1993), Daresbury Laboratory, Warrington WA4 4AD, England.
25. K. Larsen and R. Leberman, unpublished results.
26. K. Larsen and S. Perlogaes, unpublished results.
27. P. Kast and H. Hennecke, *J. Mol. Biol.* **222**, 99 (1991).
28. H. Belrhali, A. D. Yaremchuk, M. A. Tukalo, S. Cusack, unpublished results.
29. M. Carson, *J. Mol. Graphics* **5**, 103 (1987).
30. S. Cusack, M. Härtlein, R. Leberman, *Nucleic Acids. Res.* **19**, 3489 (1991); L. Ribas de Pouplana, D. D. Buechter, M. W. Davis, P. Schimmel, *Prot. Sci.* **2**, 2259 (1993) for the revised alignment of AlaRS in motif 2.

31. We thank R. Fourme and J.-P. Benoit for assistance with diffraction measurements at LURE and all our colleagues who were involved with the first protein crystallography experiments on the TROIKA beamline at the ESRF. Supported in part by NATO collaborative Research Grant 920692 (A.Y., M.T., S.C.). The coordinates have been deposited in the protein data bank, Brookhaven (1SER R code 4; 1SES seryl hydroxamate SNP; 1SET 5/O/N seryl).

27 September 1993; accepted 24 January 1994

Slow Repair of Pyrimidine Dimers at *p53* Mutation Hotspots in Skin Cancer

Silvia Tornaletti and Gerd P. Pfeifer*

Ultraviolet light has been linked with the development of human skin cancers. Such cancers often exhibit mutations in the *p53* tumor suppressor gene. Ligation-mediated polymerase chain reaction was used to analyze at nucleotide resolution the repair of cyclobutane pyrimidine dimers along the *p53* gene in ultraviolet-irradiated human fibroblasts. Repair rates at individual nucleotides were highly variable and sequence-dependent. Slow repair was seen at seven of eight positions frequently mutated in skin cancer, suggesting that repair efficiency may strongly contribute to the mutation spectrum in a cancer-associated gene.

Strong experimental and epidemiological evidence links ultraviolet (UV) irradiation to the development of human skin cancer (*1, 2*). Mutations in the *p53* tumor suppressor gene have been found in a large percentage of such cancers (*3*), most being localized in exons 5 through 9, which contain conserved sequence blocks (*4*). The predominant mutations are C→T transitions and CC→TT double transitions at dipyrimidine sequences, base alterations specifically induced by UV light (*5*). These findings have implicated the *p53* gene as a critical target in UV-related malignancies.

One important step in the prevention of tumor formation is very likely the efficient removal of DNA lesions by cellular DNA repair enzymes. Repair of UV-induced lesions in mammalian cells has been studied at the level of the gene by Southern (DNA) blot techniques (*6*). It was found that repair is gene-specific (*6*) and is most efficient on the transcribed strand of active genes (*7*) because of transcription-repair coupling (*8*). Here we determine the repair rates of UV-induced cyclobu-

Beckman Research Institute of the City of Hope, Department of Biology, Duarte, CA 91010, USA.

*To whom correspondence should be addressed.

Table 1. Repair of CPDs in the human *p53* gene. Repair rates were measured at mutation hotspots in human skin cancer (M) and at surrounding positions. Each position was analyzed three times; codons 278 and 289 were analyzed twice. Results are average values with variation between experiments being about 10 to 25%. The percentage of CPDs after 24 and 48 hours was calculated from the ratio of the band intensity at those times to the band intensity at 0 hour (*20*).

DNA strand	Codon	Sequence (5′→3′)	CPDs (%) remaining after 24 hours	CPDs (%) remaining after 48 hours
Nontranscribed	151 (M)	C^CC	58	37
	177 (M)	C^CC	95	94
	191	CC^T	26	4
	194	CT^T	36	25
	195	AT^C	13	5
	196 (M)	C^CGA	67	62
	278 (M)	T^CCT	100	12
	289	CT^C	10	5
Transcribed	243	C^CAT	11	5
	245 (M)	GC^C	56	26
	248 (M)	C^CG	30	21
	249	CCT^C	6	3
	285	CT^C	2	1
	286 (M)	TT^C	23	18
	287	CT^C	3	3
	288	ATT^C	3	3
	291	CT^T	29	18
	292	TT^T	4	5
	294 (M)	CT^C	30	28